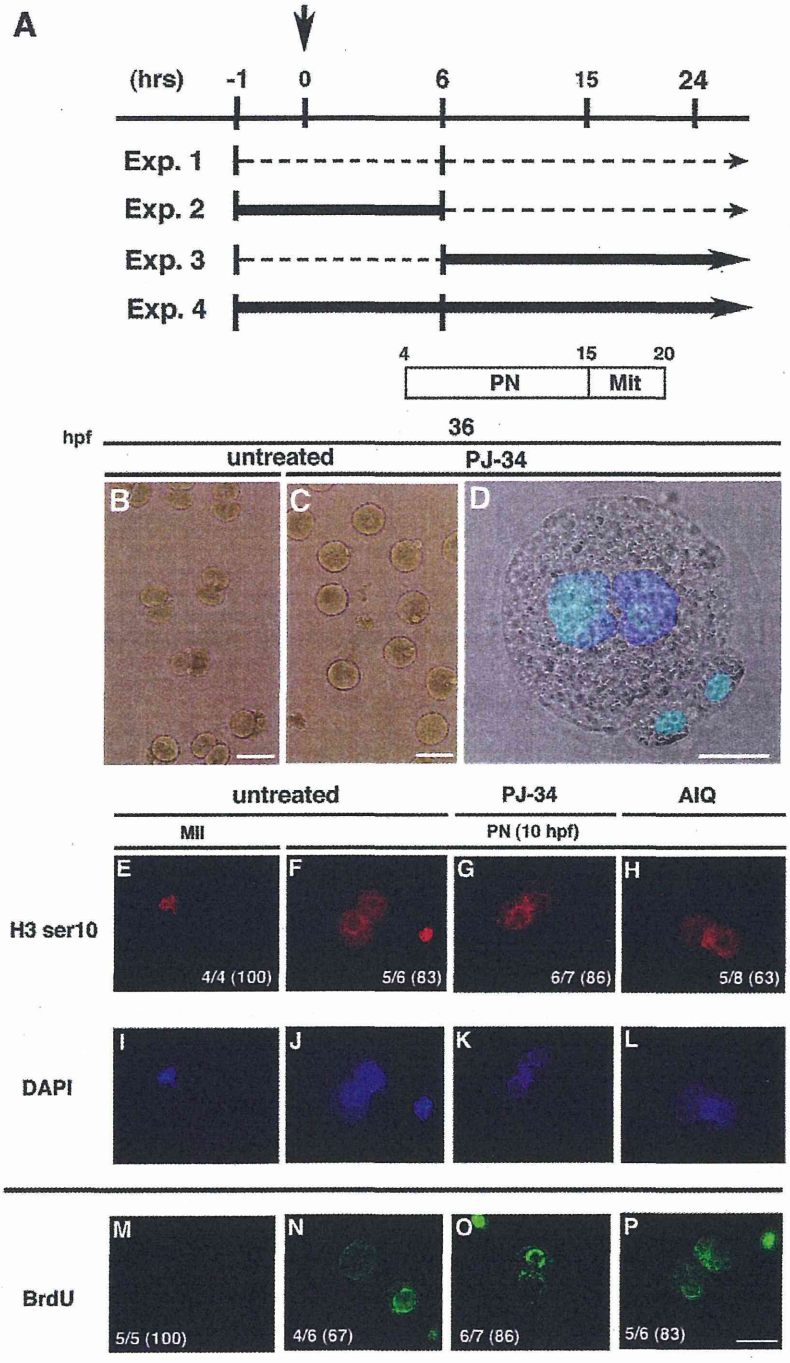

Figure 2. Inhibition of PNEB by PJ-34 and 5-AIQ. IVF and ICSI experiments were performed to assess the effects of Parp inhibitors at four different time-points during postfertilization development. (**A**) Scheme of the experimental design shows the incubation time of oocytes/embryos in normal culture medium (dotted line) or with Parp inhibitor treatment (bold line). The untreated IVF embryos reached the pronuclear stage (PN) approximately 4 hrs post-fertilization (hpf), and then underwent mitosis (Mit) from 15 to 20 hpf (open space) (**B**, **C**). Morphology of one-cell embryos at 36 hpf. Fertilized embryos were cultured for 36 hrs after insemination under untreated conditions (**B**) or with PJ-34 (**C**). A representative oocyte treated with PJ-34 shows defects in PNEB (**D**). DNA was counterstained with DAPI in blue. Immunofluorescence of untreated MII oocytes (MII) and PN embryos (PN), 30 μM PJ-34-treated, and 20 μM AIQ-treated PN embryos at 10 hpf with antibody for the phosphorylated form of histone H3 at serine 10 (H3 ser10, red) (**E–H**), and bromodeoxyuridine (BrdU, green) (**M–P**). DNA of embryos reacted with H3 ser10 antibody was counterstained with DAPI in blue (**I–L**). Frequency of the staining indicated in each panel was shown in each figure (white letters). The values in parenthesis indicate percentage of the frequency. Bars represent 25 μm.
doi:10.1371/journal.pone.0012526.g002

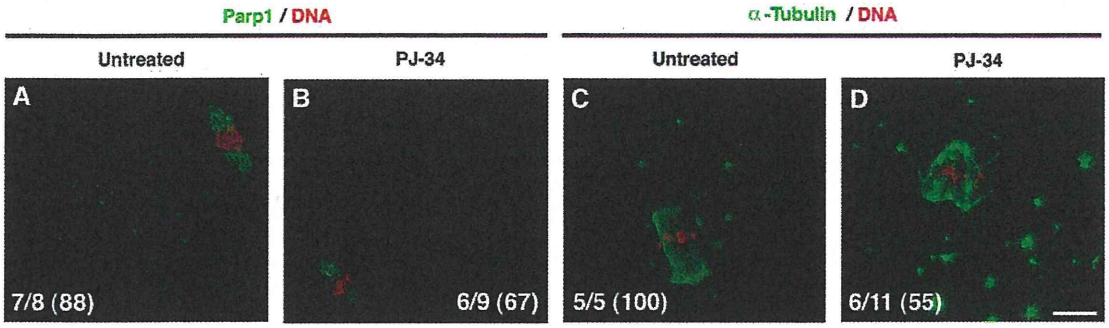

Figure 3. Parp1 expression, effects of PARylation inhibition on spindle bundle formation, PARylation on tubulins. (**A–D**) Immunofluorescence of untreated (**A, C**) and MII oocytes treated with 30 μM PJ-34 for 1 hr (**B, D**) with antibody for Parp1 (**A, B**) and a/ß-tubulin (**C, D**). Immunosignals were colored in green. DNA was counterstained with PI (red). Frequency of the indicated images was shown in each panel (white). Values in the parenthesis indicate the percentage as the frequency (**A–D**). Bar represents 20 μm. (**E, F**).
doi:10.1371/journal.pone.0012526.g003

cytoplasmic asters of MII oocytes (Figures 1A, B & 3). Administration of PJ-34 at 30 μM did not affect the localization of Parp1 at spindles (Figure 3A, B). One-hour incubation of MII oocytes in PJ-34-containing medium induced breakage of the bipolar structure of spindle bundle (untreated; 0/5 (0%), PJ-34 treated; 6/11 (55%)) with intact cytoplasmic asters (Figure 3C, D).

During postfertilization processes, immunofluorescence for a-tubulin showed that spindle between female PNs and the nucleus of the second polar body and cytoplasmic tubulins were similarly detected in both untreated and PJ-34 treated embryos (Figure 4A–H). We noticed that polynuclei of PJ-34 treated embryos were frequently detected (untreated; 2/21 (10%), PJ-34; 11/24 (45.8%), $p<0.01$). Most nuclei were connected with maternal spindles and single paternal nuclei were segregated (Figure 4B, C, F, G). These data suggest that polynuclei come from maternal genetic materials.

Identification of PARylation of a-tubulin and a defect in Erk activation in *Parp1*$^{-/-}$ oocytes

Because a-tubulin dynamics were affected by Parp inhibitors, we investigated whether a-tubulin is PARylated during the fertilization processes. For this purpose, we carried out two-dimensional gel (2D) electrophoresis followed by western blots and MALDI-TOF mass spectrometry. Western blots with the 2D electrophoresis analysis exhibited that several molecules including tubulins (a1c, §2c) were PARylated in the untreated MII oocytes (Figure 3). PARylation is suggested to be important for tubulin dynamism in the MII oocytes and a/ß-tubulins could be the potential target for PARylation.

Inhibition of the Erk phosphorylation leads to defective microtubule organization [23]. PARP1 is also reported to interact with Erk-1/2 [24,25]. Therefore, we investigated the activation of Erk 1/2 in the *Parp1*$^{-/-}$ MII oocytes. Phosphorylation of Erk-1/2

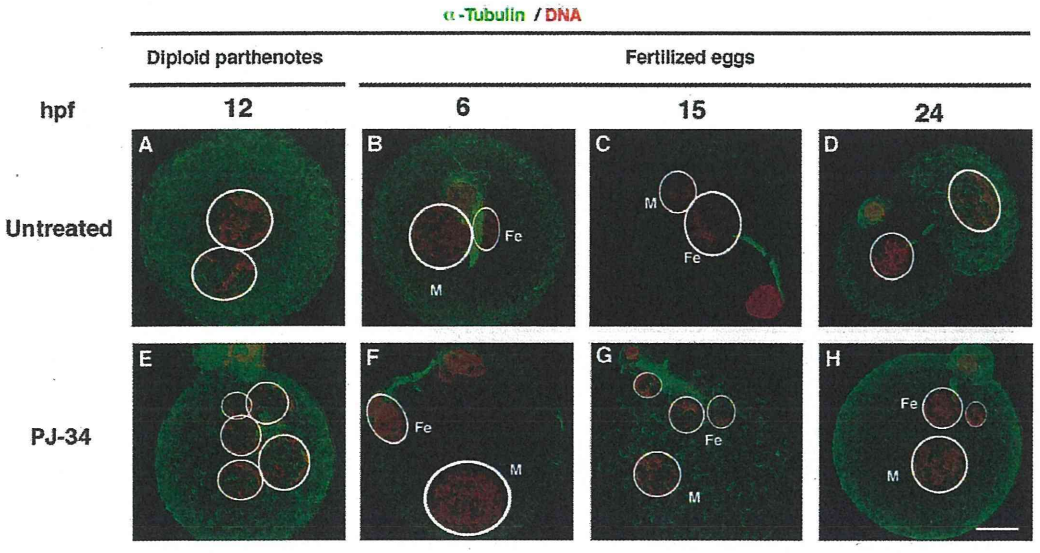

Figure 4. Effect of PARylation inhibition on spindle and polynucleation during postfertilization development. Immunofluorescence with a laser-scanning confocal microscopy of diploid parthenotes (**A, E**) and IVF embryos at 6 (**B, F**), 15 (**C, G**) and 24 (**D, H**) hpf. a-Tubulin signals were colored in green with untreated (**A–D**) and 30 μM PJ-34-treated (**E–H**) embryos. White circles represent the outlines of female (Fe) and male (M) pronuclei. DNA was counterstained with PI (red). Bar represents 20 μm (**H**).
doi:10.1371/journal.pone.0012526.g004

was down-regulated in the MII oocytes of *Parp1*$^{-/-}$ oocytes, compared with *Parp1*$^{+/+}$ oocytes, while total amount of Erk-1/2 was comparable between the genotypes (Figure 5C). However, a low level of phosphorylation of Erk is still upregulated after activation in a Parp1-independent manner. Collectively, PARylation may be important for the integrity of meiotic spindle formation mediated in part by phosphorylation regulation of Erk by Parp1 in the MII oocytes and PARylation on tubulins in the postfertilized one-cell embryos.

Defective phosphorylation of lamin by PARylation inhibition

We examined the chromosomal behavior at the late PN stage by the DNA-staining, because the pronuclear envelope was still detected in the PARylation-inhibited embryos. Condensation of chromatin was detected in non-treated one-cell embryos, whereas it was undetected in the PJ-34 treated embryos at 15 hpf stained by 4′,6-diamidino-2-phenylindole (DAPI) or propidium iodide (PI) (untreated, 28 cells in prometaphase/78 cells examined (35.9%); PJ-34 treated, 0 cells/94 cells (0%)).

Nuclear envelope breakdown is initiated by the phosphorylation of lamins [26]. We found that the lamin A and C appear to be components of the pronuclear lamina of embryos and PJ-34 treatment blocks phosphorylation of lamin A/C at 15 hpf (Figure 6A, B). Lamin A/C was largely undetectable in untreated embryos at 24 hpf, because the amount of maternal lamin A/C was reduced after the first mitosis [27]. In contrast, lamin A/C was persistently detectable in the PJ-34 treated embryos at 24 hpf, while phosphorylation of lamins was not detected (Figure 6A, B). The cdc2 kinase activity is responsible for phosphorylation of lamins [28]. Western blots revealed that between 15 hpf and 24 hpf, the phosphorylation of tyrosine 15 (Tyr15) of cdc2 (p-cdc2) was reduced in both untreated and PJ-34-treated embryos (Figure 6A). Immunocytochemistry revealed the p-cdc2 signals in the PNs of untreated and PJ-34 treated embryos (data not shown). These data suggest that the inhibition of lamin A/C phosphorylation by Parp inhibitor was not caused by affecting the activity of cdc2 kinase.

As a lamina-associated protein interacting with Parp1 [29], we examined the behavior of heterochromodomain protein 1ß (HP1ß) by immunofluorescence. A broad staining pattern of HP1ß was observed in the PNs of untreated embryos (Figure 6C). This staining pattern was reported in a previous study [30]. At 15 hpf, HP1ß signals became absent in untreated PN embryos, while a persistent localization of HP1ß was detected in PJ-34 treated

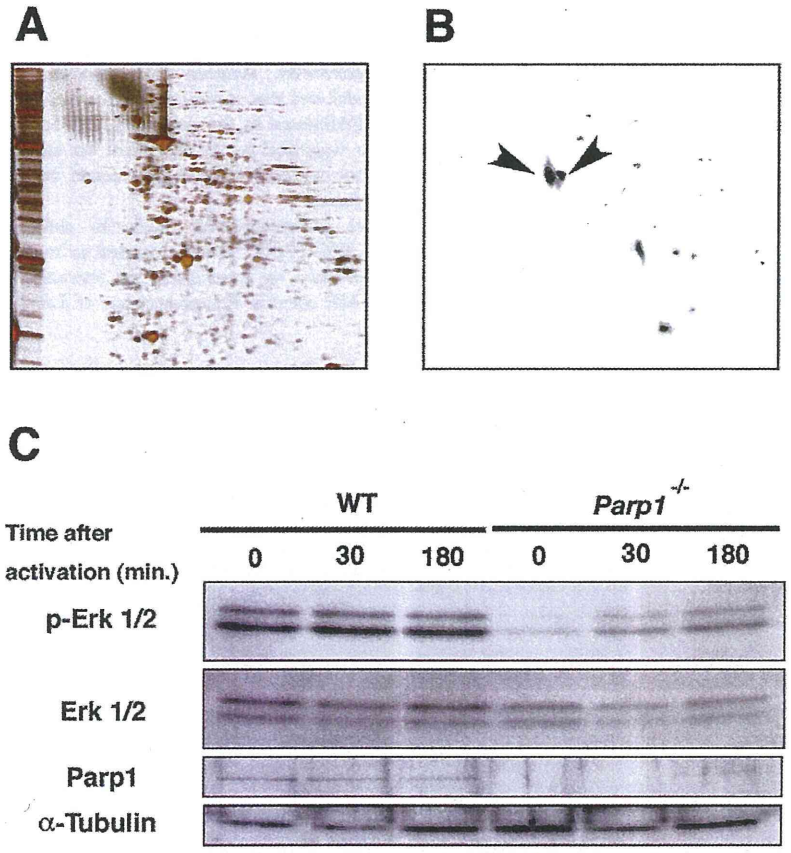

Figure 5. Biochemical analyses of PARylated proteins of MII oocytes and effects of Parp1 on the Erk-signaling. The 2D electrophoresis of 300 untreated MII oocytes with silver staining (**A**) and immunoblots with the monoclonal antibody for poly(ADP-ribose) polymers (clone 10H) (**B**). The protein spots corresponding to the immunosignals were identified as a1c (left arrowhead) and β2c (right arrowhead) tubulins by MALD-TOF mass spectrometry. (**C**) Western blotting of the protein extracts of MII oocytes of wild-type (WT) and *Parp1*$^{-/-}$ mice was performed with antibodies against the phosphorylated form of Erks (p-Erk 1/2), Erks, pan (Erk 1/2), Parp1, and a-tubulin as a control (**C**). The oocytes were collected 30 and 180 minutes after the activation of MII oocytes with Sr^{2+}. Proteins loaded in each lane corresponded to 30 oocytes.
doi:10.1371/journal.pone.0012526.g005

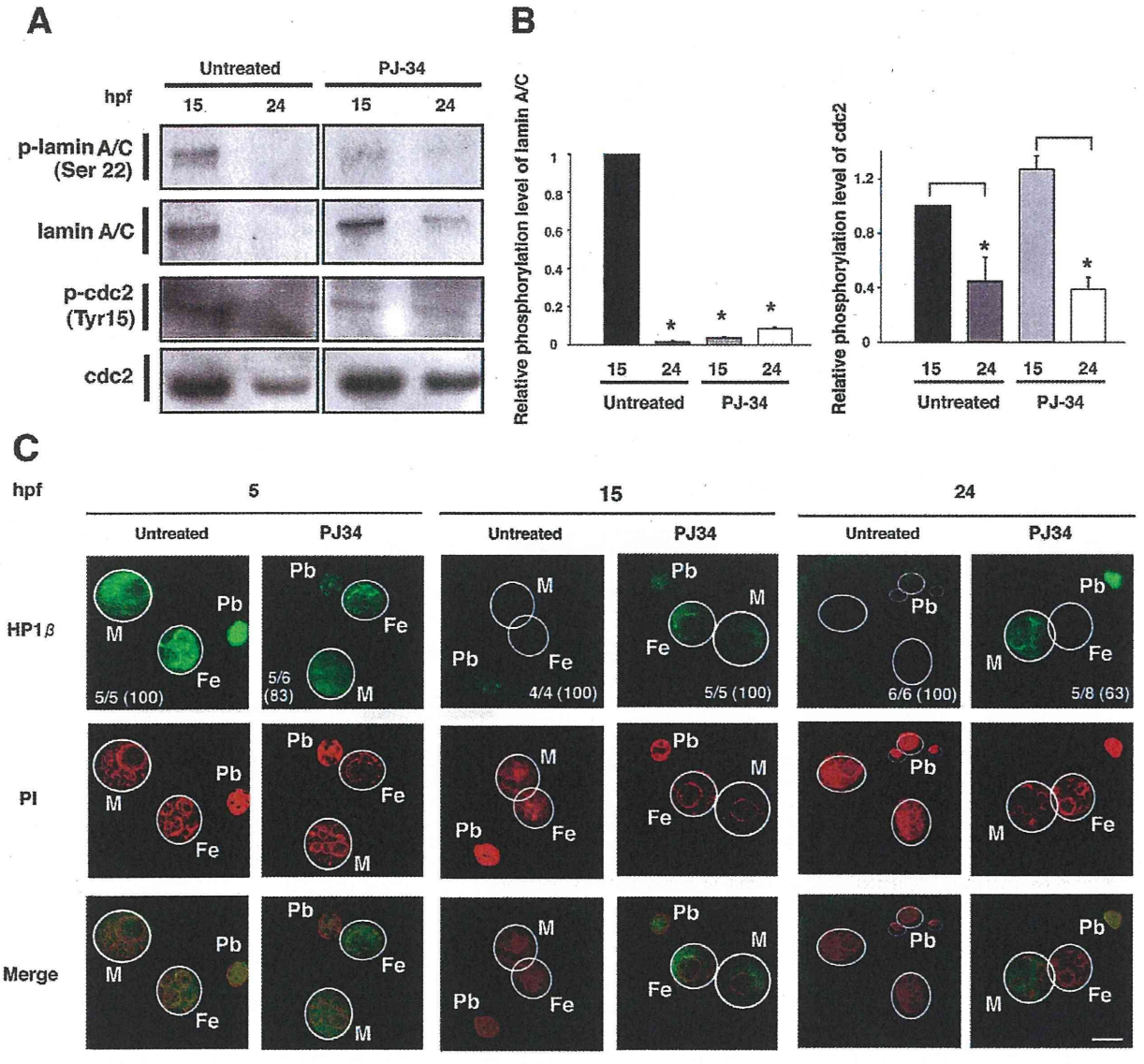

Figure 6. Defective phosphorylation of pronuclear lamins and behavior of HP1β during postfertilization development. Extracts from 100 untreated or PARylation inhibited embryos at 15 and 24 hpf were immunoblotted with antibody for phosphorylated lamin A/C, total lamin A/C, phosphorylated cdc-2, and total cdc-2 (**A**). Assessments for the relative phosphorylation levels of lamin and cdc2. Asterisks represent statistic significance (t test, $p<0.05$) (**B**). Immunofluorescence with laser-scanning confocal microscopy of untreated and PJ-34 treated embryos with antibodies for HP1β (**C**). Detected antigens were colored with green. DNA counterstained with PI was colored in red. Colocalized signals of antigens and DNA were colored in orange or yellow in merged figures. Circles (white lines) show the outlines of the female (Fe) and male (M) PNs. Other PI signals represent polar bodies (Pb). Values (percentage in parenthesis) represent frequency of the staining in each panel (**C**, upper panels). Bar represents 25 μm.
doi:10.1371/journal.pone.0012526.g006

embryos (Figure 6C). HP1ß was still detectable only in male PNs of one cell embryos by PARylation inhibition, but undetectable at the nuclei of two-cell embryos in 24 hpf embryos in the absence of PJ-34 treatment (Figure 6C). This data implies that PJ-34 delayed the HP1ß removal from chromatin of PNs and this could be involved in attenuated phosphorylation of lamin A/C.

Discussion

Our data from studies by pharmacological inhibition of PARylation in mice suggests that PARylation has three major functions in peri-fertilization processes (Figure 7). First, PARylation affects proper spindle formation in the mouse MII oocytes. Our data supports the view of Parp function described in a previous study using *Xenopus* oocytes [31]. The a/§-tubulins, which have been reported as major components of microtubules, are shown to be acceptor proteins for PARylation in mouse oocytes [32]. Our data suggest that PARylation may regulate the meiotic spindle assembly of MII oocytes either directly through PTM of tubulin, indirectly by altering MAPK signaling, or both. Immunofluorescence study showed no specific localization of PAR signals in MII-oocytes, while spindle bundle formation is

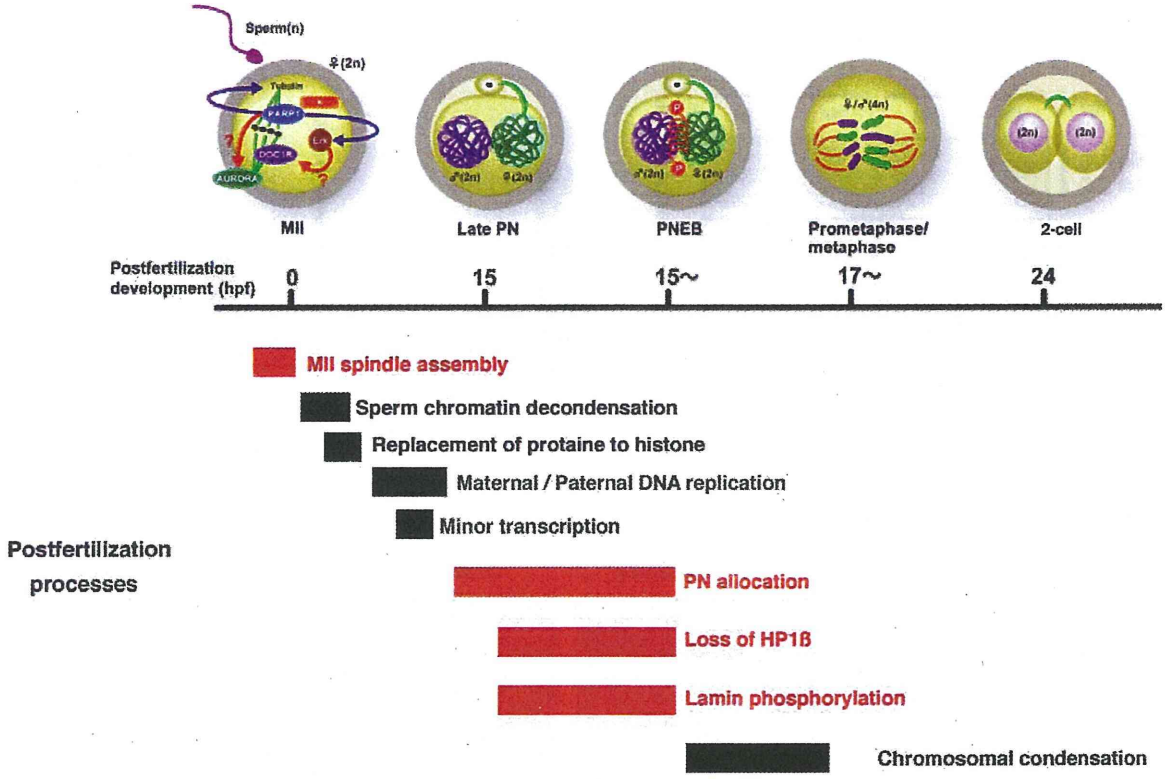

Figure 7. Scheme of spacio-temporal regulation by PARylation during perifertilization mouse development. At MII oocytes, Parp1 or other Parps are involved in spindle bundle formation mediated in part by Erk phosphorylation, which is represented as MII spindle assembly. Other Parp-associated molecules (Aurora [47]) or MAPK-associated molecules such as DOC1R [48] putatively contribute to spindle formation integrity. HP1ß loss from PNs and PN allocation are interfered by Parp inhibitors during PN stages. Phosphorylation of lamin A/C is reduced by PARylation inhibition, and subsequently PNEB is blocked. Because HP1β is associated with both chromatin and nuclear envelope, both chromatin and nuclear envelope are putatively regulated by PARylation. Duration of biological processes during 24 hrs after fertilization (open square) is listed temporally and those marked in red have been suggested to be regulated by PARylation from this study.
doi:10.1371/journal.pone.0012526.g007

perturbed by PARylation inhibition. Cytoplasmic tubulins are broadly present in mouse oocytes and associated with Erk and kinesins. Cytoplasmic Parp1 is associated with microtubule mediated by kinesins and modulates Erk signaling in neurons [24,25,33]. Our data shows downregulation of phosphorylation of Erk-1/2 in *Parp1*$^{-/-}$ MII oocytes. Collectively, we speculate that Parp1 may act as an activator of Erk-1/2 phosphorylation in the MII oocytes. Spindle bundle formation could be also regulated by other tubulin-associated Parps (Figure 6). Related to this view, interaction of tankyrase-1 with NuMA as an acceptor protein of poly(ADP-ribose) was reported to regulate mitotic spindle assembly [34]. Phosphorylation of Erks is downregulated in *Parp1*$^{-/-}$ eggs before and after activation. However, it seems that a low level of Parp1-independent phosphorylation of Erk is induced after activation, although Erk signaling is gradually inactivated upon fertilization in normal development. The PAR signals induced on meiotic spindles for a brief period during postfertilization development suggest that spindle-associated Parp1 is activated, that could mediate the Erk-signaling upon fertilization.

Intracytoplasmic Ca^{2+} release stimulates the NAD metabolism after binding of sperm to the egg cell membrane [35]. Parp catalyzes PARylation of proteins using NAD with production of nicotinamide. Thus, we speculate a novel possibility that PARylation functions as a mediator of NAD signals upon fertilization.

Second, the inhibition of PARylation results in the complete inhibition of PNEB. Mechanism of PNEB remains largely unknown. The phosphorylation of nuclear lamins is a major process in PNEB. Here, we showed that the phosphorylation of lamins A and C is hampered by the inhibition of PARylation. Interestingly, although the cdc2 kinase activity is responsible for the phosphorylation of the lamin meshwork, our data indicates that these activities are intact in PJ-34-treated embryos. Lamin A negatively affects epigenetic regulation of the myogenin gene expression in mouse myoblasts [36]. Synthesis of lamin A is absent during the cleavage-stage blastomere [37] and in stem cells [38]. Recently, Parp1 was found to co-localize with HP1 that promotes the interaction of heterochromatin with the inner layer of the nuclear envelope [29]. We found that, in contrast to untreated embryos, HP1ß signals were persistently detected in the male PNs of PJ-34-treated embryos at 24 hpf. Together with the evidence from a previous study describing that PARylation also functions in telomere regulation [39], our data raise the possibility that PARylation functions as a regulatory machinery of the pronuclear envelope disassembly.

Our data using PJ-34 and 5-AIQ was different from those obtained with 3-aminobenzamide (3-AB) [22]. We found that IVF

experiments and *in vitro* culture of one-cell embryos with 5 mM 3-AB did not show any influence on the transition of the first mitotic cleavage. In this study, we did not observe the inhibition of PAR activation at the PN stage by 5 mM 3-AB (data not shown). Our immunofluorescence showed residual signals of PAR at the PNs of embryos treated with 5 mM 3-AB, but barely with PJ-34 and 5-AIQ. Collectively, we found that PJ-34 or 5-AIQ, water-soluble PARP inhibitors, are more suitable for a more precise assessment of inhibition of total PARylation activity at postfertilization development. Further analyses will be needed to seek for the functional PARPs, which regulate MII spindle assembly, signal transduction of PNEB processes during early stages of postfertilization development.

Recently, PARylation inhibitors emerge as effective therapeutic agents for mammary tumors [40]. Our study also implicates a risk of subfertility by administrating PARP inhibitors. Furthermore this study raises a possibility of PARP inhibitors as potent contraceptive chemicals. Molecular dissection of the PARylation system will provide our understanding for significance of PTM in mammalian development [41].

Materials and Methods

Oocyte and embryo manipulations

Parp1$^{-/-}$ mutant mice under a B6D2F1 hybrid background were generated by sequential backcrosses of *Parp1*$^{+/-}$ mice to C57BL/6J and DBA2/J [11]. Oocytes were collected from superovulated B6D2F1 females 14 hrs after the intraperitoneal injection of equine chorionic gonadotropin (eCG), followed by the injection of human chorionic gonadotropin (hCG). For IVF, oocytes were cultured in TYH medium [42]. Sperm was collected from the caudal epididymis of B6D2F1 males and incubated in TYH medium. After the preincubation of MII oocytes in 200/300 μL of TYH medium with or without PJ-34 or 5-AIQ as described in Table 1, sperm (150 sperm/μL) was added to the oocytes. Intracytoplasmic sperm injection (ICSI) was carried out essentially as described previously [43]. ICSI was carried out in Hepes-buffered CZB medium with or without 30 μM PJ-34. Thereafter, embryos were cultured in modified Whitten medium [44].

Animal care

All animals were housed according to the institutional guidelines in compliance with National Institutes of Health guidelines. Experiments using animals were approved by the Animal Care and Use committee of Mitsubishi Kagaku Institute of Life Sciences, MITILS, and National Cancer Center Research Institute (T05-026-MB06, T05-026-CB07).

Antibodies

The antibodies and dilutions used in this study were described in Supplemental Table S1. The HRP–conjugated rat or rabbit IgG (1:10000, Jackson Immunoresearch Laboratory) and HRP-conjugated mouse IgG (1:1000, Bio-Rad) as the secondary antibodies for immunodetection and the Alex Fluor conjugates (1:200, Invitrogen) of IgG for immunofluorescence.

Immunofluorescence

The cumulus-oocyte complex was dissociated by hyaluronidase (Sigma) and the zona pellucida was removed with 0.5% actinase (Kaken, Japan). After incubation of the denuded oocytes or embryos for at least 30 minutes, the oocytes or embryos were placed into fibrin clots [45]. The fibrin clots were prepared by mixing 1 μl fibrinogen (12.5 mg/ml PBS: Calbiochem) with 1 μl thrombin (10 mg/ml distilled H_2O: Sigma). For the staining of microtubules, oocytes and embryos were permeabilized by microtubule stabilizing buffer (60 mM PIPES, 25 mM HEPES, 10 mM EGTA, 2 mM $MgCl_2$, adjusted to pH 6.9) for 3 minutes, and then fixed with 3% formaldehyde for 10 minutes at 37°C. The cells were incubated with primary antibodies for 1 hr or overnight at 37°C, followed by incubation with blocking buffer (PBS containing 5% normal goat serum and 0.05% Tween-20). The cells were then incubated with secondary antibodies for 1–2 hrs at 37°C. After washing with PBS, the cells were counterstained with PI and subjected to microscopic analyses. For the staining with histone modification antibodies, the cells were fixed with 4% paraformaldehyde for 15 minutes at 4°C and then permeabilized with PBS containing 0.1% BSA and 0.5% TritonX-100 for 10 minutes. The cells were incubated with primary antibodies overnight at 4°C, and then with secondary antibodies for at least 3 hrs at 4°C. For detection of DNA synthesis, the IVF embryos at 8 hpf were transferred to Whitten medium containing 10 μM 5-bromo-2′-deoxyuridine (BrdU, Roche Diagnostic Corporation) and incubated for 2 hrs. Embryos were then fixed and permeabilized as described above. After washing for three times, embryos were incubated in culture medium containing 2 N HCl for 30 min. Embryos were washed for 5 times with borate buffer (pH 8.5) and then for 3 times with PBS. Neutralized embryos were incubated for 30 min with PBS containing 5% FBS, and then reacted with anti-bromodeoxyuridine monoclonal antibody (Roche Diagnostic Corporation) overnight at 4°C. The images were captured under a light microscopy (Axiophot, Zeiss) or confocal microscopy (IX71 with Fluoview FV300, Olympus) system.

Immunoblots

For the two-dimensional gel electrophoresis, oocyte extracts were collected into sample buffer (7 M urea, 2 M thio-urea, 4% CHAPS, 40 mM DTT, 2% IPG buffer (pH 3–10) (GE Healthcare), protease inhibitor cocktail). Samples were purified using the 2D Clean-UP kit (GE Healthcare). Protein extracts corresponding to 300 MII oocytes or one-cell embryos were applied to an Immobiline drystrip (pH 3–10, GE Healthcare) and subjected to isoelectric focusing with a multiphor apparatus (GE Healthcare) as the first protein separation. The stripe was then applied to a 10% SDS-PAGE gel for the second protein separation. The proteins on the gels were transferred to a BioTrace nitrocellulose membrane for histones WB (pore size, 0.2 μm, Pall) or Immobilon PVDF membrane (Millipore), and reacted with primary antibodies for 1 hr at room temperature. The membrane was washed and then reacted with secondary HRP-conjugated antibodies (see below). The signals were enhanced by Can Get Signal, an immunoreaction enhancer solution (Toyobo) and detected with the Chemi-Lumi One kit (Nacalai) and Amersham Hyperfine ECL (GE Healthcare).

Parg analysis

Eggs in the Parg buffer (20 mM potassium phosphate (pH 7.5), 0.1% Triton X-100, 10 mM §-mercaptoethanol) were mixed for 30 minutes at 4°C by a mixer, and then subjected to freezing and thawing five times. Aliquots of the extracts corresponding to 2 eggs were used for the thin layer chromatography (TLC) assay. Fifteen nanograms of recombinant GST-Parg (0.3 μL) were used as control. Extracts were incubated for 2 hrs at 25°C with ^{32}P-labeled PAR. The reactions were terminated by adding 0.1% SDS. The samples were spotted on a polyethylene impregnated cellulose TLC plate (Macherht-Nagal), developed with a developing buffer [46], and then detected by BAS2500 (Fuji Film).

RT-PCR

Total RNA was isolated from 100–150 MII oocytes using Sepasol-RNA I Super (Nacalai). The cDNA was synthesized by Superscript III (Invitrogen) according to the manufacturer's instructions. The PCR reactions were carried out at 55 and 60°C as the annealing temperature with 30 and 40 cycles. The primer sequences used in this study and expected length of amplified cDNA fragments were described in Table S2.

Supporting Information

Table S1 The primary antibodies used in this study.
Found at: doi:10.1371/journal.pone.0012526.s001 (0.13 MB TIF)

Table S2 The primer sequences to detect *Parps*, *Parg*, and *G3pdh* genes by RT-PCR.

Found at: doi:10.1371/journal.pone.0012526.s002 (9.44 MB TIF)

Acknowledgments

We thank Dr. I. Kitabayashi, Dr. T. Jenuwein, and Dr. T. Takeuchi for providing antibodies and plasmids, and Dr. T. Sugimura, Dr. R. Yanagimachi, Dr. K. Yanagida, and Dr. K. Naito for their informative insights and suggestions, and Miss R. Umeda, and Miss K. Oda for technical assistance.

Author Contributions

Conceived and designed the experiments: TO MM. Performed the experiments: TO HO TH SI AO. Analyzed the data: TO HO MM. Contributed reagents/materials/analysis tools: TH KN AO TN MM. Wrote the paper: TO MM.

References

1. Yanagimachi R (1994) Mammalian fertilization. In: Knobil E, Neil JD, eds. Physiology of Reproduction. 2nd edition. New York: Raven Press. pp 189–317.
2. Florman H, Ducibella T (2007) Mammalian fertilization. In: Neil JD, P.M. Wassarman PM, eds. Knobil and Neill's Physiology of Reproduction. 3rd edition. Amsterdam, Netherlands: Elsevirer. pp 55–112.
3. Rawe VY, Olmedo SB, Nodar FN, Ponzio R, Sutovsky P (2003) Abnormal assembly of annulate lamellae and nuclear pore complex coincides with fertilization arrest at the pronuclear stage of human zygotic development. Hum Reprod 18: 576–582.
4. Telford NA, Watson AJ, Schultz GA (1990) Transition from maternal to embryonic control in early mammalian development: a comparison of several species. Mol Reprod Dev 26: 90–100.
5. Fan HY, Sun QY (2004) Involvement of mitogen-activated protein kinase cascade during oocyte maturation and fertilization in mammals. Biol Reprod 70: 535–547.
6. Vignon X, Zhou Q, Renard JP (2002) Chromatin as a regulative architecture of the early developmental functions of mammalian embryos after fertilization or nuclear transfer. Cloning Stem Cells 4: 363–377.
7. Santos F, Peters AH, Otte AP, Reik W, Dean W (2005) Dynamic chromatin modifications characterize the first cell cycle in mouse embryos. Dev Biol 280: 225–236.
8. Schultz RM (1993) Regulation of zygotic gene activation in the mouse. Bioassay 15: 531–538.
9. Sugimura T, Miwa M (1994) Poly(ADP-ribose): historical perspective. Mol Cell Biochem 138: 5–12.
10. Schreiber V, Dantzer F, Ame JC, de Murcia G (2006) Poly(ADP-ribose): novel functions for an old molecule. Nat Rev Mol Cell Biol 7: 517–528.
11. Masutani M, Suzuki H, Kamada N, Watanabe M, Ueda O, et al. (1999) Poly(ADP-ribose) polymerase gene disruption conferred mice resistant to streptpzptpcin-induced diabetes. Proc Natl Acad Sci U S A 96: 2301–2304.
12. Menissier de Murcia J, Ricoul M, Tartier L, Niedergang C, Huber A, et al. (2003) Functional interaction between PARP-1 and PARP-2 in chromosome stability and embryonic development in mouse. EMBO J 22: 2255–2263.
13. Koh DW, Lawler AM, Poitras MF, Sasaki M, Wattler S, et al. (2004) Failure to degrade poly(ADP-ribose) causes increased sensitivity to cytotoxicity and early embryonic lethality. Proc Natl Acad Sci U S A 101: 17699–17704.
14. Abdelkarim GE, Gertz KK, Harms C, Katchanov J, Dirnagl U, et al. (2001) Protective effects of PJ-34, a novel, potent inhibitor of poly(ADP-ribose) polymerase (PARP) *in vitro* and *in vivo* models of stroke. Int J Mol Med 7: 255.
15. McDonald MC, Mota-Filipe H, Wright JA, Abdelrahman M, Threadgill MD, et al. (2000) Effects of 5-aminoisoquinolinone, a water-soluble, potent inhibitor of the activity of poly(ADP-ribose) polymerase on the organ injury and dysfunction caused by hemorrhagic shock. Br J Pharmacol 130: 843–850.
16. Erdelyi K, Kiss A, Bakondi E, Bai P, Szabo C, et al. (2005) Gallotannin inhibits the expression of chemokines and ainflammatory cytokines in A549 cells. Mol Pharmacol 68: 895–904.
17. Huang D, Yang C, Wang Y, Liao Y, Huang K (2009) PARP-1 suppresses adiponectin express9oin through poly(ADP-ribosyl)ation of PPAR gamma in cardiac fibroblasts. Cardiovasc Res 81: 98–107.
18. Bakondi E, Bai P, Szabo EE, Hunyadi J, Gergely P, et al. (2002) Detection of poly(ADP-ribose) polymerases activation in oxidatively stressed cells and tissues using biotinylated NAD substrate. J Histochem Cytochem 50: 91–98.
19. Valdor R, Schreiber V, Saenz L, Martinez T, Munoz-Suano A, et al. (2008) Regulation of NFAT by poly(ADP-ribose) polymerase activity in T cells. Mol Immunol 45: 1863–1871.
20. Fossati S, Cipriani G, Moroni F, Chiarugi A (2007) Neither energy collapse nor transcription underlie in vitro neurotoxicity of poly(ADP-ribose) polymerase hyper-activation. Neurochem Int 50: 203–210.
21. Inbar-Rozensal D, Castiel A, Visochek L, Castel D, Dantzer F, et al. (2009) A selective eradication of human nonhereditary breast cancer cells by phenanthridine-derived polyADP-ribose polymerase inhibitors. Breast Cancer Res 11: R78.
22. Imamura T, Neildez TM, Thenevin C, Paldi A (2004) Essential role for poly(ADP-ribosyl)ation in mouse preimplantation development. BMC Mol Biol 5: 4.
23. Tong C, Fan HY, Chen DY, Song XF, Schatten H, et al. (2003) Effects of MEK inhibitor U0126 on meiotic progression in mouse oocytes: microtubule organization, asymmetric division and metaphase II arrest. Cell Res 13: 375–383.
24. Kauppinen TM, Chan WY, Suh SW, Wiggins AK, Huang EJ, et al. (2006) Direct phosphorylation and regulation of poly(ADP-ribose) polymerase-1 by extracellular signal-regulated kinases 1/2. Proc Natl Acad Sci USA 103: 7136–7141.
25. Cohen-Armon M, Visochek L, Roensal D, Kalal A, Geistrikh I, et al. (2007) DNA-independent PARP-1 activation by phosphorylated ERK2 increases Elk1 activity: a link to histone acetylation. Mol Cell 26: 297–308.
26. Gerace L, Blobel G (1980) The nuclear envelope lamina is reversibly depolymerized during mitosis. Cell 19: 277–287.
27. Schatten G, Maul GG, Schatten H, Chaly N, Simerly C, et al. (1985) Nuclear lamins and peripheral nuclear antigens during fertilization and embryogenesis in mice and sea urchins. Proc Natl Acad Sci U S A 82: 4727–4731.
28. Peter M, Nakagawa J, Doree M, Labbe JC, Nigg EA (1990) *In vitro* disassembly of the nuclear lamina and M phase-specific phosphorylation of lamins by cdc2 kinase. Cell 61: 591–602.
29. Quenet D, Gasser V, Fouillen L, Cammas F, Sanglier-Cianferani S, et al. (2008) The histone subcode: poly(ADP-ribose) polymerase-1 (Parp-1) and Parp-2 control cell differentiation by regulating the transfcriptional intermediary factor TIF beta and heterochromatin protein HP1alpha. FASEB J 22: 3853–3865.
30. Arney KL, Bao S, Bannister AJ, Kouzarides T, Surani MA (2002) Histone methylation defines epigenetic asymmetry in the mouse zygotes. Int J Dev Biol 46: 317–320.
31. Chang P, Jacobson MK, Mitchison TJ (2004) Poly(ADP-ribose) is required for spindle assembly and structure. Nature 432: 645–649.
32. Satchell MA, Zhang X, Kochanek PM, Dixon CE, Jenkins L, et al. (2003) A dual role for poly-ADP-ribosylation in spatial memory acquisition after traumatic brain injury in mice. J Neuroses 85: 697–708.
33. Midorikawa R, Takei Y, Hirokawa N (2006) KIF4 motor regulates activity-dependent neuronal survival by suppressing PARP-1 enzymatic activity. Cell 125: 371–383.
34. Chang P, Coughlin M, Mitchison TJ (2009) Interaction between Poly(ADP-ribose) and NuMA contributes to mitotic spindle pole assembly. Mol Biol Cell 20: 4575–4585.
35. Epel D, Patton C, Wallace RW, Cheung WY (1981) Calmodulin activates NAD kinase of sea urchin eggs: an early event of fertilization. Cell 23: 543–549.
36. Hakelien AM, Delbarre E, Kristine G, Gaustad KG, Berndia B, et al. (2008) Expression of the myodystrophic R453W mutation of lamin A in C2C12 myoblasts causes promoter-specific and global epigenetic defects. Exp Cell Res 314: 1869–1880.
37. Clarke HJ (1992) Nuclear and chromatin composition of mammalian gametes and early embryos. Biochem Cell Biol 70: 856–866.
38. Pajerowski JD, Dahl KN, Zhong FL, Sammak PJ, Discher DE (2007) Physical plasticity of the nucleus in stem cell differentiation. Porc Natl Acad Sci USA 104: 15619–15624.
39. Smith S, Giriat I, Schmitt A, de Lange T (1998) Tankylase, a poly(ADP-ribose) polymerase at human telomere. Science 282: 1484–1487.
40. Fong PC, Boss DS, Yap TA, Tutt A, Wu P, et al. (2009) Inhibition of poly(ADP-ribose) polymerase in tumor from BRCA mutation carriers. N Engl J Med 361: 123–134.
41. Sims RJ, 3rd, Reinberg D (2008) Is there a code embedded in proteins that is based on post-translational modifications? Nat Rev Mol Cell Biol 9: 815–820.

42. Toyoda Y, Yokoyama M, Hoshi T (1971) Studies on the fertilization of mouse eggs in vitro. J Anim Reprod 16: 147–151.
43. Osada T, Toyoda A, Moisyadi S, Akutsu H, Hattori M, et al. (2005) Production of inbred and hybrid transgenic mice carrying lathe (>200 kb) foreign DNA fragments by intracytoplasmic sperm injection, Mol Reprod Dev 72: 329–335.
44. Whitten WK, Biggers JD (1968) Complete development in vitro of the pre-implantation stages of the mouse in a simple chemically defined medium. J Rrprod Fertil 17: 399–401.
45. Simerly C, Schatten G (1993) Techniques for localization of specific molecules in oocytes and embryos. Methods Enzymol 225: 516–553.
46. Shimokawa T, Masutani M, Nagasawa S, Nozaki T, Ikota N, et al. (1999) Isolation and cloning of rat poly(ADP-ribose) glycohydrolase: presence of a potential nuclear export signal conserved in mammalian orthologs. J Biochem 126: 748–755.
47. Monaco L, Kolthur-Seetharam U, Loury R, Murcia JM, de Murcia G, et al. (2005) Inhibition of Aurora-B-kinase activity by poly(ADP-ribosyl)ation in response to DNA damage. Proc Natl Acad Sci U S A 102: 14244–14248.
48. Terret ME, Lefebvre C, Djiane A, Rassinier P, Moreau J, et al. (2003) DOC1R: a MAP kinase substrate that control microtubule organization of metaphase II mouse oocytes. Development 130: 5169–5177.

Exp. Anim. 60(1), 57–63, 2011

—Original—

Kyoto Rhino Rats Derived by ENU Mutagenesis Undergo Congenital Hair Loss and Exhibit Focal Glomerulosclerosis

Takashi KURAMOTO[1)], Mitsuru KUWAMURA[2)], Fumi TAGAMI[1)], Tomoji MASHIMO[1)], Masato NOSE[3)], and Tadao SERIKAWA[1)]

[1)]Institute of Laboratory Animals, Graduate School of Medicine, Kyoto University, Sakyo-ku, Kyoto 606-8501, [2)]Laboratory of Veterinary Pathology, Osaka Prefecture University, Izumisano, Osaka 598-8531, and [3)]Department of Pathogenomics, Graduate School of Medicine, Ehime University, Toon, Ehime 791-0295, Japan

Abstract: *N*-ethyl-*N*-nitrosourea (ENU) mutagenesis is an important tool for studying gene function and establishing human disease models. Here, we report the characterization of a novel hairless mutant rat strain that carries a recessive mutation called Kyoto rhino (*krh*), which was created by ENU-mutagenesis. We produced a F344-*krh* strain through inbreeding without backcrossing to F344 rats. The *krh*/*krh* rats lost their coat hair by eight weeks of age. They also developed wrinkled skin, cystic hair canals and long curved nails by four months of age. Markedly dilated hair follicles that contained keratin debris were observed during histological analysis of the skin. The *krh* locus was mapped near the hairless (*Hr*) gene on chromosome 15. Sequence analysis revealed a nonsense mutation (c. 1238 C>A, p. S413X) in the *Hr* gene. The truncated HR protein was deduced to lack a zinc-finger domain and repression domains. In aged Hr^{krh}/Hr^{krh} rats, focal glomerulosclerosis (FGS) was observed in which collapsed glomeruli contained protein exudates in Bowman's capsule. Mesangial matrices that had proliferated in segments and foot processes that were fused in podocytes were also observed. The Hr^{krh}/Hr^{krh} rats also suffered from significant proteinuria. Given its breeding history, the F344-Hr^{krh} strain may harbor ENU-induced mutation(s) that underlie FGS in addition to having the Hr^{krh} mutation. The F344-Hr^{krh} rat is a useful model of skin disease and may provide a new model system for the examination of the pathogenesis of FGS.

Key words: disease model, hairless, mutation, nephrosis

Introduction

Hairless mutant rodents are valuable models for studying molecular mechanisms that underlie hair growth control. They are particularly valuable when searching for the genetic basis of hereditary human hair disorders.

In mice, 43 mutations are responsible for primary genetic hairlessness [7]. Among them, the most important are allelic mutations of the hairless (*Hr*) gene. The best characterized allele is the hairless (*hr*). Hr^{hr}/Hr^{hr} mice have a striking total alopecia phenotype which appears between three and four weeks of age. The pheno-

(Received 17 August 2010 / Accepted 16 September 2010)

Address corresponding: T. Kuramoto, Institute of Laboratory Animals, Graduate School of Medicine, Kyoto University, Yoshidakonoe-cho, Sakyo-ku, Kyoto 606-8501, Japan

type originates in the periorbital region and propagates in a wave-like fashion in the rostral-to-caudal direction [20]. It has been determined, through comparative studies of several distinct mouse *Hr* mutations, that the *Hr* gene product plays a key role in controlling hair follicle transformation during the catagen phase [20]. The hairless phenotype of *Hr*-mutant mice (Hr^{hr}/Hr^{hr}) is similar to that of the human disease atrichia. The disease phenotype comprises papular lesions (APL) and alopecia universalis congenital (ALUNC), complete hair loss after birth. It is a result of human *HR* mutation [2, 4, 9].

Another important mutant *Hr* of the mouse is the rhino (*rh*) mouse. Hr^{rh}/Hr^{rh} mice lose all of their hair by seven weeks of age, possess wrinkled skin and their nails overgrow. Additionally, they develop an autoimmune disease characterized by hypergammaglobulinemia, immunoglobulin deposits in the basement membrane of skin, spleen, liver, and kidney, and the presence of antinuclear antibodies which appear in young mice and increase with age [14].

Several rat hair loss mutations have been described. They are for the Charles River hairless rat [1], the Iffa Credo (IC) rat [6], the Hairless Wistar Yagi rat also known as the HWY/Slc rat [13], the Dundee experimental bald rat also known as the DEBR rat [22], the Bald rat [12], and the Hirosaki hairless rat (HHR) [17]. An intragenic deletion in the desmoglein 4 gene underlies the IC rat skin phenotype [6]. The absence of 80-kb of genomic DNA that contains five basic keratin genes is the cause of the HHR rat hairless phenotype [17].

Rat hair follicles are larger than those of mice. Therefore hairless mutant rats are attractive models for studying hair follicle development, differentiation, and cycling. Rat mutants are also good models for evaluating the effects of new drugs for treating human skin diseases. Therefore, it would be beneficial to establish new hairless rat models for these purposes.

We recently treated rats with *N*-ethyl-*N*-nitrosourea (ENU) to obtain different mutants [16]. Several hair loss phenotypes were identified by employing phenotype-driven screening. A hair loss mutant line was established by crossing mutant-type males with wild-type female littermates. Our analysis of the breeding record of this line can be used to prove that the hair loss phenotype is autosomal recessive. Thus, the mutation was named Kyoto rhino (*krh*).

In this study, we identified the *krh* mutation using a positional candidate approach and characterized the *krh/krh* rats. *krh* is a nonsense mutation of the rat *Hr* gene. *krh/krh* rats develop renal failure with massive proteinuria and focal glomerulosclerosis (FGS).

Materials and Methods

Animals

ENU-treated F344/NSlc male rats were mated with F344/NSlc female rats to generate G_1 offspring [16]. The ENU-mutagenized G_1 rats (n=42) were used as founders for the phenotype-driven screening of recessive mutations. Briefly, the G_1 rats were crossed with two F344 rats to generate G_2 offspring. The female G_2 offspring were then backcrossed with their parental G_1 rats to generate G_3 offspring. The recessive mutations induced by ENU in the G_1 rats become homozygous in the G_3 rats. Among the G_3 offspring (n=11) from a G_1 male (#E2307), three rats showed a hair loss phenotype; these rats were probands (P generation). We mated the affected rats with the normal littermates to fix the hair loss phenotype. The phenotype was fixed at the F_2 generation and the mutation was called *krh*. A mutant line was established by employing brother-sister mating (homozygous male × heterozygous female). The generation of inbreeding had reached F_6 at the end of August, 2010. The animal care and experimental procedures that were used were approved by the Animal Research Committee, Kyoto University and were carried out according to the Regulation on Animal Experimentation at Kyoto University.

Genetic mapping

Twenty N_2 rats were produced from a (BN/SsNSlc × F344-*krh/krh*)F_1 × F344-*krh/krh* backcross. The genotypes for the *krh* locus were identified on the basis of coat phenotype at four to five weeks of age. Genomic DNA was prepared from tail biopsies using an automatic DNA purification system (PI-200, Kurabo, Japan) and genotypes for *D15Rat10*, *D15Rat13*, and *D15Rat85* were determined. Linkage relationship was evaluated using the chi-square test of the Excel statistical package.